Tectonophysics - Elsevier Publishing Company, Amsterdam
Printed in The Netherlands

USE OF MICROEARTHQUAKES IN THE STUDY OF THE MECHANICS OF EARTHQUAKE GENERATION ALONG THE SAN ANDREAS FAULT IN CENTRAL CALIFORNIA[1]

J.P. EATON, W.H.K. LEE and L.C. PAKISER

U.S. Geological Survey, National Center for Earthquake Research, Menlo Park, Calif. (U.S.A.)

(Received December 17, 1969)

SUMMARY

A small, dense network of independently recording portable seismograph stations was used to delineate the slip surface associated with the 1966 Parkfield-Cholame earthquake by precise three dimensional mapping of the hypocenters of its aftershocks. The aftershocks were concentrated in a very narrow vertical zone beneath or immediately adjacent to the zone of surface fracturing that accompanied the main shock. Focal depths ranged from less than 1 km to a maximum of 15 km.

The same type of portable network was used to study microearthquakes associated with an actively creeping section of the San Andreas fault south of Hollister during the summer of 1967. Microearthquake activity during the 6-week operation of this network was dominated by aftershocks of a magnitude-4 earthquake that occurred within the network near Bear Valley on July 23. Most of the aftershocks were concentrated in an equidimensional region about 2½ km across that contained the hypocenter of the main shock. The zone of the concentrated aftershocks was centered near the middle of the rift zone at a depth of about 3½km. Hypocenters of other aftershocks outlined a 25 km long zone of activity beneath the actively creeping strand of the fault and extending from the surface to a depth of about 13 km.

A continuing study of microearthquakes along the San Andreas, Hayward, and Calaveras faults between Hollister and San Francisco has been under way for about 2 years. The permanent telemetered network constructed for this purpose has grown from about 30 stations in early 1968 to about 45 stations in late 1969. Microearthquakes between Hollister and San Francisco are heavily concentrated in narrow, nearly vertical zones along sections of the Sargent, San Andreas, and Calaveras faults. Focal depths range from less than 1 km to about 14 km.

[1]Work done in cooperation with the Division of Reactor Development and Technology, U.S. Atomic Energy Commission. Publication authorised by the Director, U.S. Geological Survey.

INTRODUCTION

For the last 3½ years, the National Center for Earthquake Research (N.C.E.R.) of the U.S. Geological Survey has been using the natural field laboratory provided by the San Andreas fault in central California to develop techniques for mapping microearthquakes to study the mechanics of earthquake generation. This report will describe the outstanding features of the natural laboratory, outline the microearthquake studies, and summarize the principal results obtained from them.

PRINCIPAL FEATURES OF THE CENTRAL CALIFORNIA FIELD LABORATORY AREA

In the scheme of the "New Global Tectonics," Isacks, et al., 1968, the San Andreas fault is a transform fault along which the Pacific plate is sliding northwestward with respect ot the Americas plate (Wilson, 1965; Morgan, 1968; Le Pichon, 1968; Fig.1). Details of its termination near the

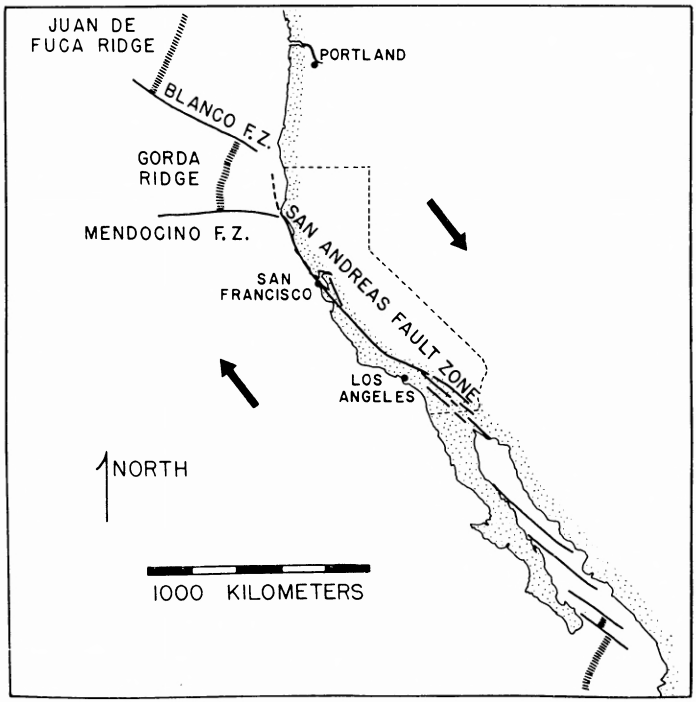

Fig.1. Global tectonic setting of the San Andreas fault system. Heavy arrows indicate the relative movement between the Pacific and Americas plates that is accommodated by right-lateral strike-slip displacement along the San Andreas fault system in California and northern Mexico.

head of the Gulf of California on the south (Sykes, 1968; Larsen et al., 1968) and on or between the Mendocino and Blanco fracture zones on the north (Bolt et al., 1968) have not yet been resolved. The cumulative right-lateral strike-slip offset along the San Andreas fault in central California since Cretaceous time must be measured in hundreds of kilometers (Hill and Dibblee, 1953; Wentworth, 1968).

The largest historic earthquakes on the San Andreas fault system accompanied long surface fault breaks that extended into the central California region now under intensive study by N.C.E.R. (Fig.2). During the 1857

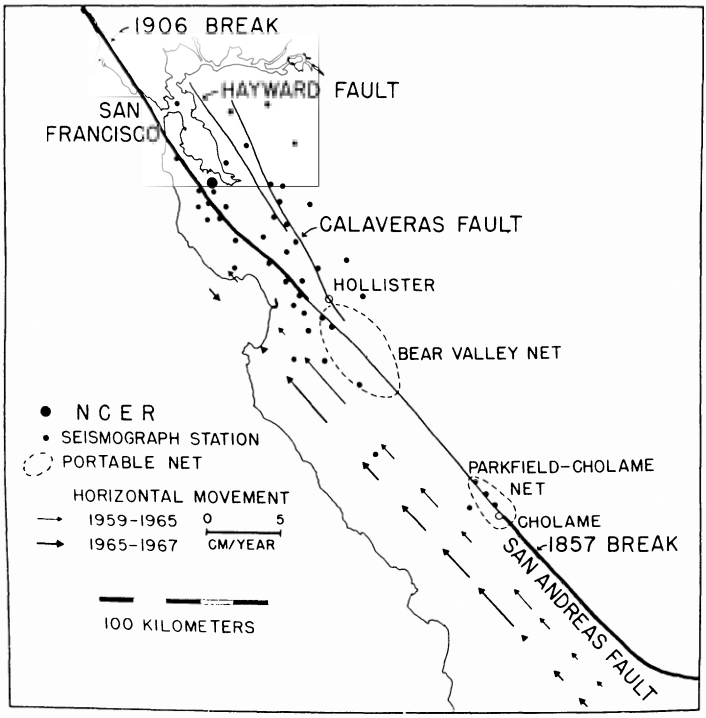

Fig.2. Location map of principal study areas and N.C.E.R. seismic networks along the San Andreas and related faults in central California. Individual stations of the telemetered network recorded at N.C.E.R. are indicated by closed circles, and areas covered temporarily by dense networks of portable stations during special studies are outlined by dashed lines. Sections of the San Andreas fault that ruptured during the great earthquakes of 1906 (San Francisco) and 1857 (Fort Tejon) are marked by heavy lines. Open circles indicate locations of towns mentioned in text.

Displacement velocities of points on the southwest side of the San Andreas fault relative to points on the northeast side, determined by repeated measurements of geodimeter lines extending diagonally across a 5–15 km wide strip along the fault, are shown by vectors with solid heads (after Hofmann et al., 1968).

Fort Tejon earthquake, the fault broke from the vicinity of Cholame for a distance of more than 300 km southeastward across the Transverse Ranges, north of Los Angeles; and during the 1906 San Francisco earthquake, it broke from the vicinity of Hollister for a distance of more than 400 km northwestward to the vicinity of Cape Mendocino, at the landward end of the Mendocino fracture zone (Fig.1). In both cases, the fault offset was strike-slip in a right-lateral sense and averaged several meters over the length of the breaks. The section of the San Andreas fault between these two great breaks has produced many small to moderately large earthquakes (up to magnitudes of 6.5) but no great ones.

The current level of microearthquake activity is very low along the two sections of the fault that have produced the great historic earthquakes; yet it is high between Hollister and Cholame where no great earthquake has occurred. Thus, regional frequency–magnitude relationships based on short-term microearthquake observations are of limited use for identifying regions that will experience great earthquakes and for estimating their recurrence intervals (Allen et al., 1965).

For about 10 years it has been recognized that the active central section of the fault has been undergoing nearly steady creep, with the rocks on the southwest side of the active fault trace sliding northwestward relative to those on the northeast side (Tocher, 1960; Steinbrugge and Zacher, 1960). The average rate of creep in this region is about 2 cm/year and rates as high as 5 cm/year have been observed locally (Tocher, 1966; R.O. Burford and W.T. Kinoshita, written personal communication, 1969). Creep diminishes toward the southeast and dies out altogether in the region of the 1857 break southeast of Cholame. It also diminishes toward the northwest and does not penetrate significantly into the region of the 1906 break on the San Andreas. Analyses of offsets in structures such as fences and roads indicate that the pattern of creep now being observed on the San Andreas fault has been sustained for many decades (Brown and Wallace, 1968).

Although little or no creep has been observed on the section of the San Andreas fault northwest of Hollister, evidence for slow, probably intermittent creep along the eastern branch of the system (Hayward and Calaveras faults) has been found at many localities (Radbruch et al., 1966; Radbruch, 1968; Rogers and Nason, 1968).

Repeated measurements of the lengths of long geodimeter lines that cross the San Andreas fault diagonally show a relative northwestward motion of the southwest side with respect to the northeast side at rates of as much as 4 cm/year (Fig.2) in the region between San Francisco and the Transverse Ranges (curve in the fault at the bottom of Fig.2). North of Hollister, accumulation of strain across the San Andreas fault is slow; but across the whole system (San Andreas, Hayward, Calaveras faults), it appears to be nearly the same as across the San Andreas fault alone southeast of Hollister (Hofmann et al., 1968).

The strain rate measured by the geodimeter lines across a 5–15 km wide strip along the fault is about twice that accounted for by creep on the active trace alone. This discrepancy suggests that creep may affect only the upper part of the crust and that elastic strain that might be released in a future large earthquake is accumulating at a greater depth.

Detailed studies of microearthquakes have been undertaken along three sections of the San Andreas fault in central California; (1) between Hollister and San Francisco, in the region where the Calaveras and Hayward faults branch off the San Andreas; (2) in the region around Bear Valley, southeast of Hollister, where the rate or creep along the fault is large; and (3) between Parkfield and Cholame, where the zone of microearthquake activity and creep ends against the quiet section of the 1857 break. In the work at Bear Valley and at Parkfield–Cholame, dense temporary networks of independently recording portable seismographs were used, whereas the work between Hollister and San Francisco has been carried out by means of a network of telemetered seismograph stations that are recorded at N.C.E.R. (Fig.2).

The portable seismograph stations have been described by Eaton et al. (1969). Their magnification curve (Fig.3) peaks at a much higher frequency,

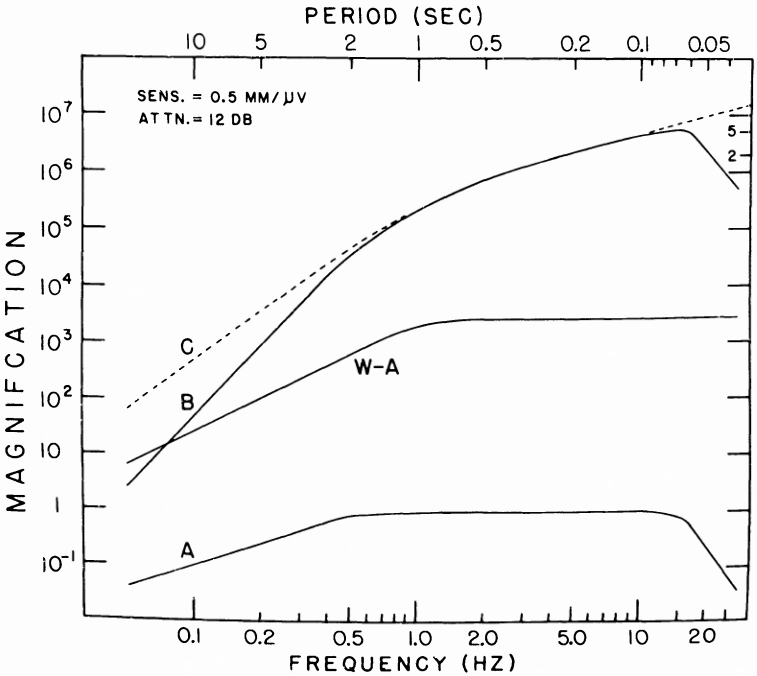

Fig.3. Portable seismograph station response. Curve A = relative voltage amplification of the combined recording and playback equipment; curve C = relative voltage output from a critically damped EV-17 seismometer subjected to constant amplitude sinusoidal ground motion; curve B = overall system magnification for a record/reproduce sensitivity of 0.5 mm/μvolt; curve W–A = magnification curve for the standard Wood–Anderson seismograph.

15 c.p.s., than those of conventional short-period seismographs used in local earthquake studies, and they can be operated at very high magnifications at quiet sites. A seismogram of a microearthquake recorded near its epicenter is shown in Fig.4.

The response of the telemetered seismograph stations is similar to that of the portable stations. Their signals are recorded in groups of 14 stations on 16-mm film strip recorders to facilitate reduction and analysis of the data. Errors in the timing of sharp wave onsets should not exceed 0.03 sec for either type of station.

The fundamental approach in the N.C.E.R. microearthquake program has been to determine precise hypocenters for large numbers of microearthquakes so that the active seismogenic structures can be identified and mapped in three dimensions. Consequently, dense networks of seismographs covering and surrounding the structures under study are needed. Special calibration shots or short seismic-refraction profiles made in order to determine the local crustal structure may also be required, particularly if the network is not sufficiently redundant to detect serious flaws in the crustal model used for hypocenter determinations.

Hypocenters were determined on the Geological Survey's IBM 360/65 computer by the program HYPOLAYR (Eaton, 1969). A first estimate of the hypocenters is adjusted by Geiger's method to minimize the sum of the squares of the residuals of observed arrival times with respect to those computed from an earth model consisting of flat-lying layers of constant velocity over a half-space. Adjustment of the focal parameters (X_0, Y_0, Z_0 and t_0) is continued until the average residual, mean deviation of the residuals, and change in mean deviation of the residuals from one iteration to the next all become smaller than prescribed test values or until an iteration limit is exceeded.

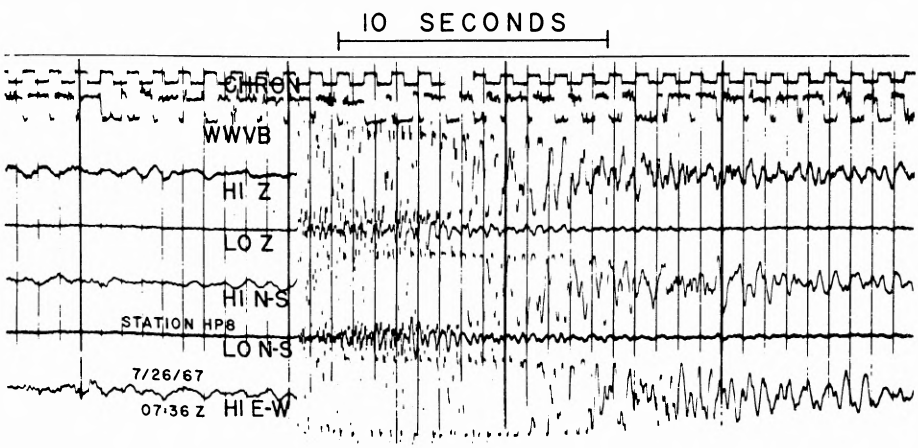

Fig.4. Playback from a 3-component portable seismograph station of a magnitude 0.5 microearthquake with a focal depth of about 2.5 km that originated at an epicentral distance of 6 km from the station.

Results from the San Francisco Bay area telemetered seismic network

A year-long effort to install and test an effective telemetered short-period seismic net and to develop efficient methods of reducing the data was culminated in early 1968 with the completion of an operating 30-station microearthquake network concentrated between the south end of San Francisco Bay and Hollister (Fig.5). In its original conception, this network

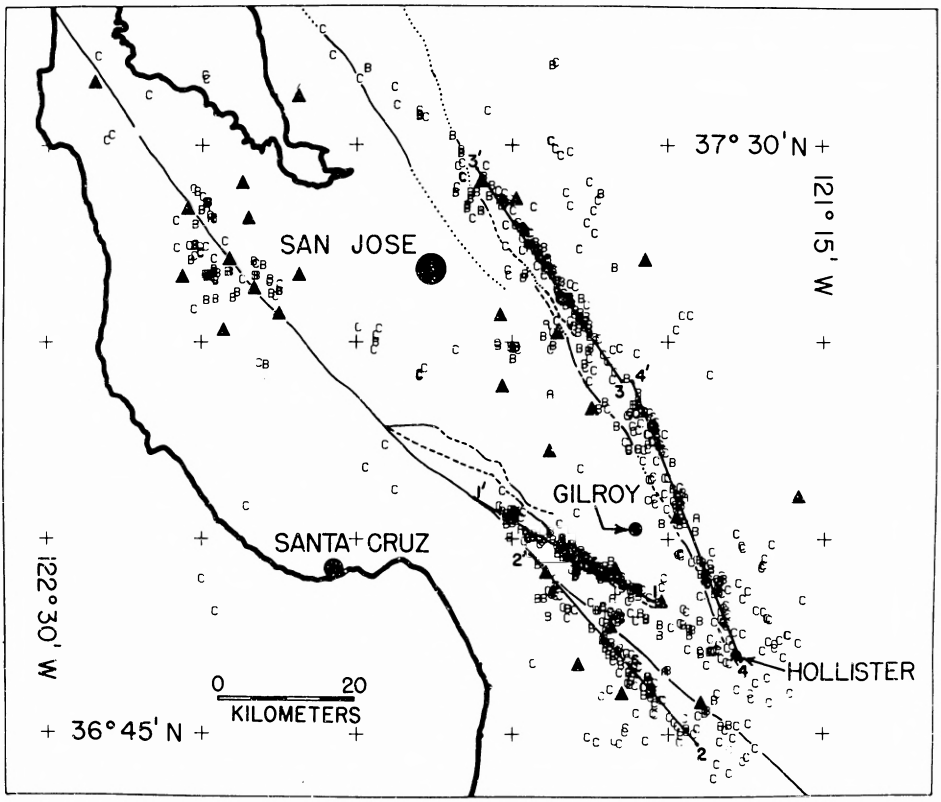

Fig.5. Epicenters of well recorded events within the telemetered network from March 1968 through April 1969. Plotted symbols indicate the reliability of hypocenter determinations: *A*, well determined epicenter (± 1 km) and focal depth (± 2 km); *B*, fairly well determined epicenter (± 2.5 km) and focal depth (± 5 km); and *C*, moderately well determined epicenter (± 5 km) but undetermined focal depth. Zones of hypocenter concentrations marked off by the numbered lines are as follows: *1–1'*, Sargent fault; *2–2'*, San Andreas fault west of Hollister; *3–3'*, Calaveras fault, northern section; *4–4'*, Calaveras fault, southern section.

consisted of three separate clusters to provide detailed coverage of three critical parts of this region. The first was centered on the "locked" section of the San Andreas fault at the south end of the San Francisco peninsula; the second was centered on the southeastern end of the 1906 break west of Hollister, where it appears the creep along the fault dies out; and the third was along the Calaveras fault north of Hollister. It soon was apparent that the three clusters provided good coverage of microearthquakes throughout the region, and additional stations have been added subsequently to fill in the weaker portions of the original network.

In the routine analysis of records for the period March 1968 through April 1969, epicenters were obtained for about 2,000 microearthquakes that originated in or near the Bay area network. Epicenters for about half of these events were not well established because they occurred outside the network or because they were very small and were recorded by only a few stations. Following a suggestion of Prof. Bruce Bolt, of the University of California (Berkeley), the individual earthquake hypocenter determinations were given quality ratings, and only well located events were used in the analysis of the distribution of hypocenters. Two groups of criteria were used in rating the hypocenters: (1) mean deviation of the residuals and size of the estimated errors in focal parameters; (2) the number of stations available for the solution, the epicentral distance to the nearest station, and the maximum gap in the azimuthal coverage provided by available stations.

In this system *A* denotes an event with well determined epicenter ($\pm$ 1 km) and focal depth ($\pm$ 2 km), *B* denotes an event with fairly well determined epicenter ($\pm$ 2.5 km) and focal depth ($\pm$ 5 km), *C* denotes an event with a moderately well determined epicenter ($\pm$ 5 km) but with an undetermined focal depth, and *D* denotes an event with poorly determined epicenter or with fewer than 6 stations available for the hypocentral calculation. Microearthquakes with *A*, *B*, and *C* hypocenter quality ratings are plotted in Fig. 5. Epicenters are concentrated primarily in three zones: (1) on the Sargent fault (*1–1'*) southwest of Gilroy; (2) just west of the surface trace of the San Andreas fault west of Hollister (*2–2'*); and (3) along a curved line about 2 km east of the surface trace of the Calaveras fault northwest of Hollister (*3–3'* and *4–4'*). These zones form a continuous N-shaped pattern in which activity on the Sargent fault connects the northwestern limit of concentrated activity along the San Andreas fault to the southeastern limit of concentrated activity along the Calaveras fault.

Reference planes were fitted to the *A* and *B* quality hypocenters in in 5 km wide strips centered on each of the lines *1–1'*, *2–2'*, *3–3'*, and *4–4'* to minimize the sum of the squares of the horizontal deviations of the hypocenters from the fitted planes. Events that lay more than 2 standard deviations from the fitted planes on the first fitting were weighted zero and the planes were refitted to the remaining hypocenters. Transverse and longitudinal sections of the hypocenters in regions *1–1'*, *2–2'*, and *3–3'* were prepared by projecting the hypocenters onto vertical planes that were perpendicular and parallel, respectively, to the surface traces of the fitted planes.

The reference plane fitted to the 179 *A* and *B* quality hypocenters along the Sargent fault (line *1–1'*, Fig.5) strikes N61°W and dips 85° northeast; and the standard deviation of hypocenters from the reference plane is 0.6 km. In the southeastern half of the zone, hypocenters are concentrated in the depth range 2–8 km, with none deeper than 10 km; and in the north-

western half of the zone they are concentrated at depths of 8–14 km, with none shallower than 6 km nor deepr than 15 km (Fig.6).

The reference plane fitted to the 57 *A* and *B* quality hypocenters along the San Andreas fault west of Hollister (line *2–2'*, Fig.5) strikes N41°W and dips 83° toward the southwest; and the standard deviation of hypocenters is 0.8 km. Hypocenters are practically confined to the depth range of 0–7 km along the southeastern three quarters of the zone, but they descend to 6–13 km along the northwestern quarter of the zone (Fig.7).

The reference plane fitted to the 80 *A* and *B* quality hypocenters along the northern section of the Calaveras fault hypocentral zone (line *3–3'*, Fig.5) strikes N35°W and dips 85° to the northwest; and the standard deviation of hypocenters from the plane is 0.5 km. Hypocenters are concentrated at depths of 0–5 km along the southeastern third of the longitudinal section and at depths of 5–10 km along the northwestern two thirds of the section (Fig.8). None is deeper than 12 km.

The reference plane fitted to the 58 *A* and *B* quality hypocenters along the southern section of the Calaveras fault hypocentral zone (line *4–4'*, Fig.5) strikes N22°W and dips 89° toward the northeast. The standard deviation of hypocenters from the fitted plane is 0.9 km.

Focal depths throughout the San Francisco Bay area network are predominantly shallow– from the surface to depths of 8 or 10 km. The deepest hypocentral zone ranges from 7 to 14 km in depth and underlies a shallower quiet zone where the active sections along the Sargent and San Andreas faults join west of Gilroy (Fig.5) and where activity along both dies off abruptly toward the northwest.

The crustal model used in the analysis of the telemetered network data was based on available seismic-refraction data and consists of four flat-lying homogeneous layers over a half-space: 3.0 km/sec from 0.0 to 1.2 km; 5.0 km/sec from 1.2 to 3.5 km; 6.0 km/sec from 3.5 to 15.0 km; 6.8 km/sec from 15.0 km to 25.0 km; and 8.05 km/sec below 25 km. A study to improve the crustal model on the basis of quarry blasts and well recorded, favorably located Bay area earthquakes is now under way.

Aftershocks of the July 23, 1967, Bear Valley earthquake

In the summer of 1967 a network of 18 portable stations was laid out along the San Andreas fault to monitor microearthquakes associated with the actively creeping section of the fault in the vicinity of Bear Valley, southeast of Hollister (Fig.2). Only a few days after the network was placed in operation, a magnitude-4 earthquake occurred near the center of the network; and during the next 6 weeks, a remarkable sequence of aftershocks of this earthquake was recorded.

Nearly 500 of the largest of approximately 3,000 aftershocks recorded on magnetic tape by seismographs on quiet sites near Bear Valley were played back on all available stations and their hypocenters were calculated. The distribution of the hypocenters is illustrated by the map (Fig.9) and by transverse and longitudinal sections prepared by projecting hypocenters onto vertical planes that are perpendicular and parallel, respectively, to the surface trace of the actively creeping strand of the fault through the region (Fig.10). About 80% of the located aftershocks were concentrated in

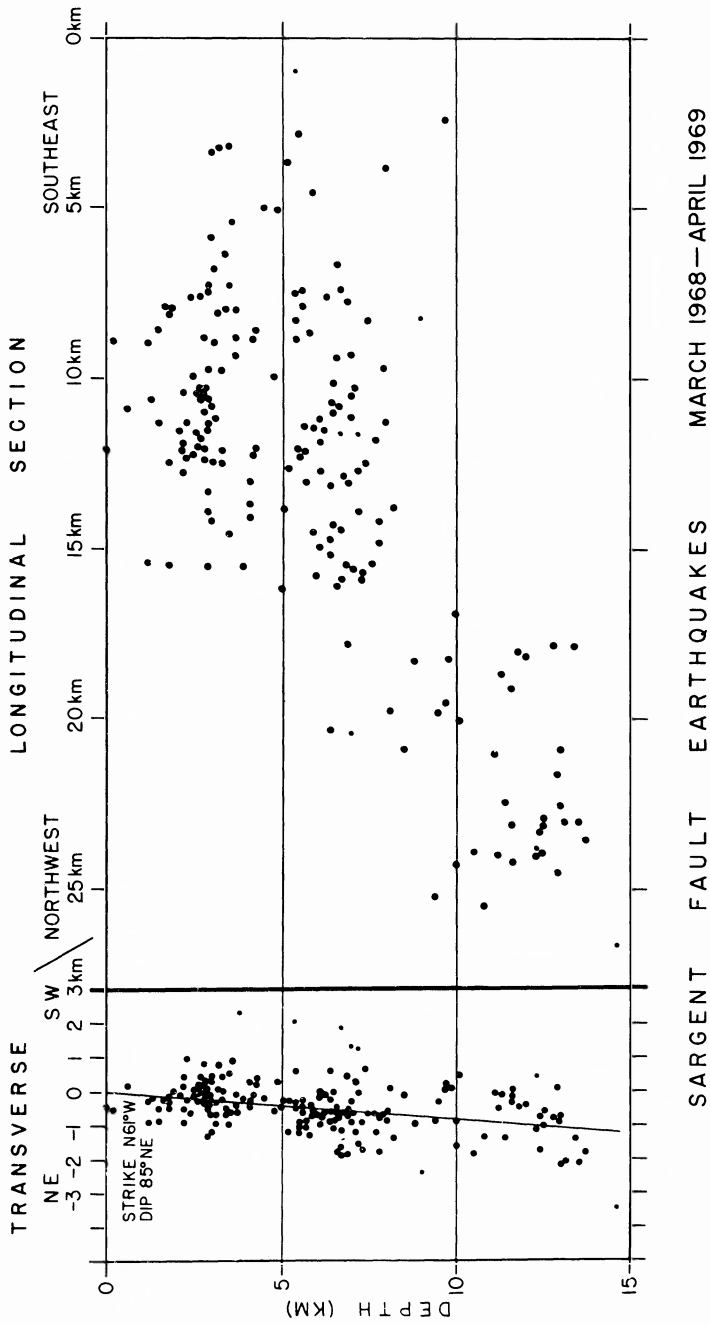

SARGENT FAULT EARTHQUAKES MARCH 1968—APRIL 1969

Fig.6. Earthquakes in the Sargent fault hypocentral zone projected onto vertical planes perpendicular (left) and parallel (right) to the surface trace of the plane fitted by least squares to the hypocenters. Events that lay more than 2 standard deviations from the fitted plane are plotted as small dots.

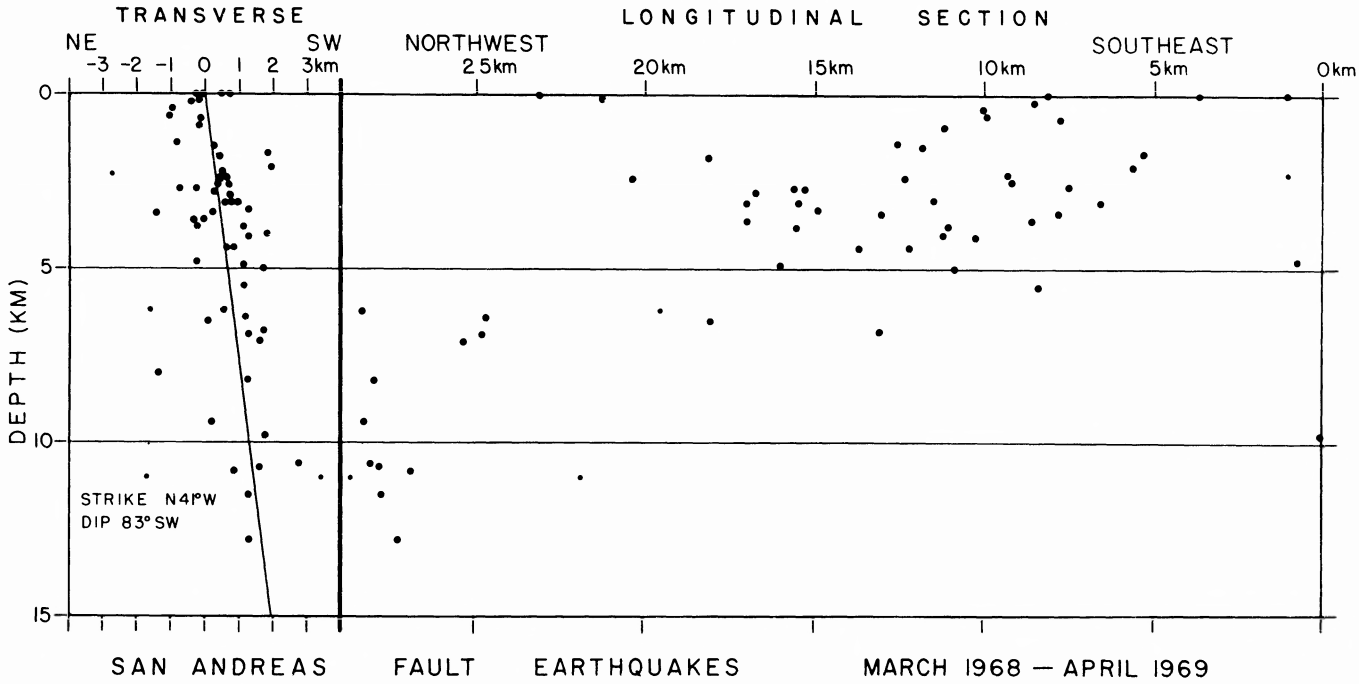

Fig.7. Earthquakes in the hypocentral zone along the San Andreas fault west of Hollister projected onto vertical planes perpendicular (left) and parallel (right) to the surface trace of the plane fitted by least squares to the hypocenters. Events that lay more than 2 standard deviations from the fitted plane are plotted as small dots.

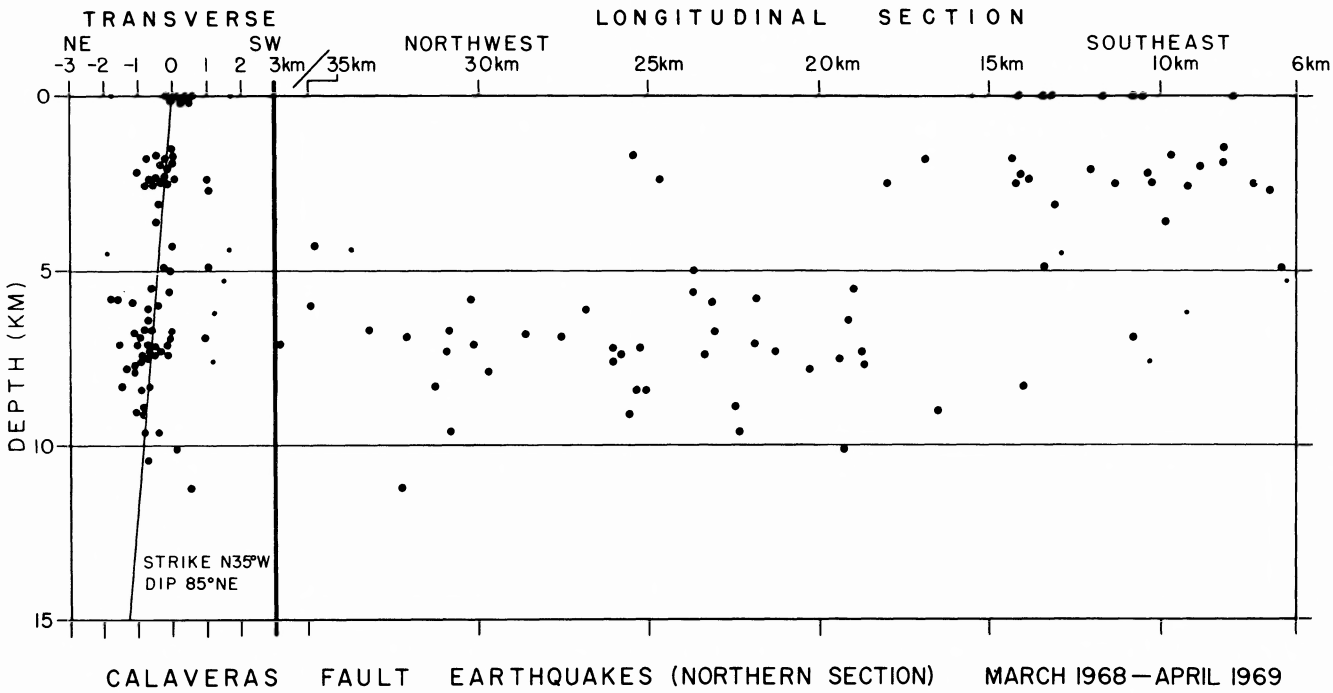

Fig.8. Earthquakes in the northern section of the Calaveras fault hypocentral zone projected onto vertical planes perpendicular (left) and parallel (right) to the surface trace of the plane fitted by least squares to the hypocenters. Events that lay farther than 2 standard deviations from the fitted plane are plotted as small dots.

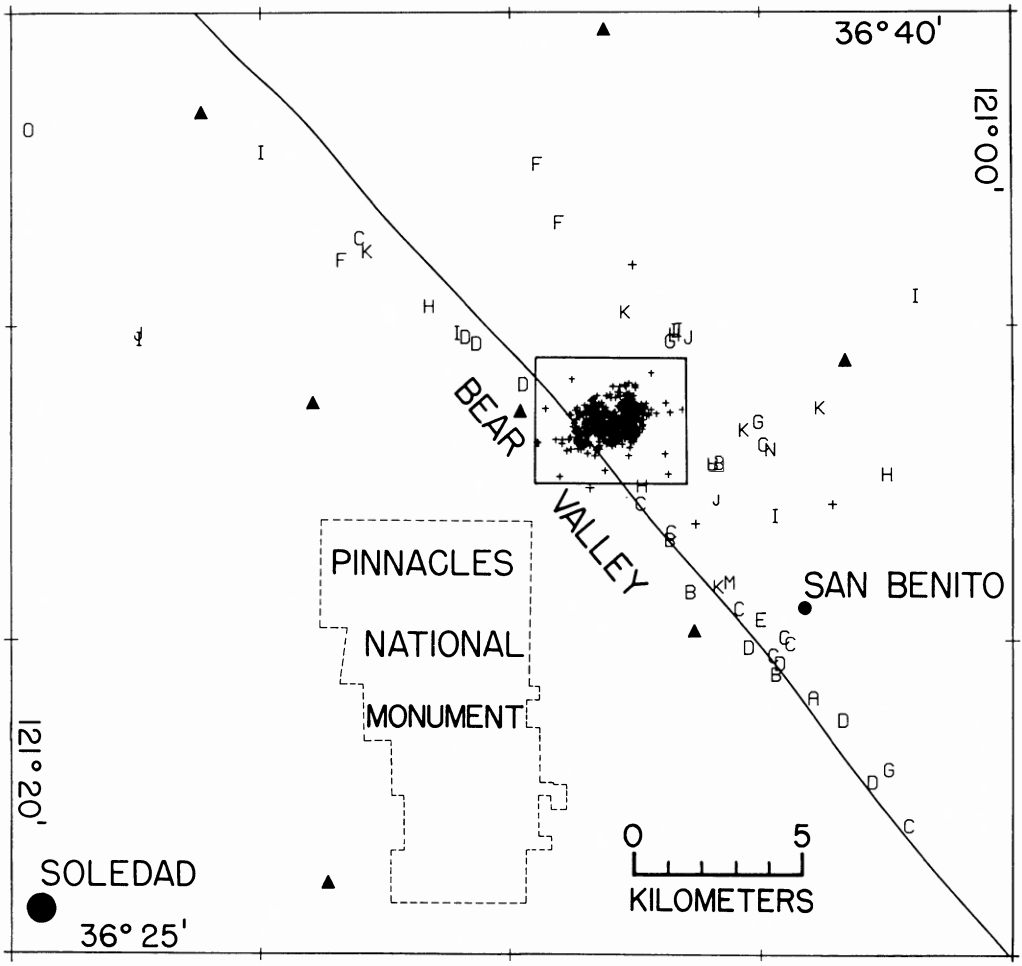

Fig.9. Aftershocks of the July 23, 1967, Bear Valley earthquake. The actively creeping trace of the San Andreas fault is shown by the solid line; but the rift zone is several km wide at Bear Valley and extends from about 1 km southwest of the active trace to about 3 km northeast of it. Portable seismograph stations are shown as solid triangles. Outside of the central rectangle, the letter symbol showing the epicenter of an earthquake also indicates its focal depth: 0–1 km = *A*, 1–2 km = *B*, and so on; a large cross indicates a shallow event for which a reliable depth could not be calculated. Inside the central rectangle hypocenters were very closely spaced (more than 300 of them), and they are plotted as small crosses.

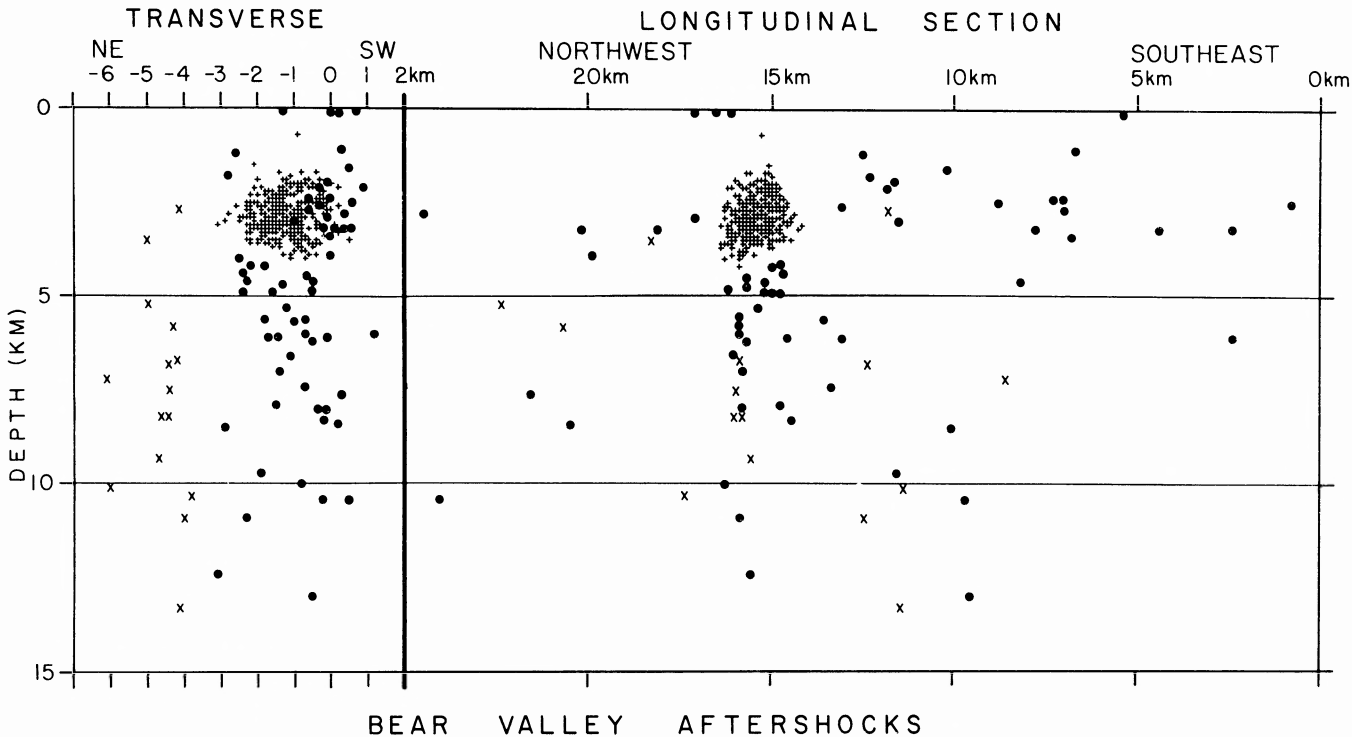

Fig.10. Bear Valley aftershocks projected onto vertical planes perpendicular (left) and parallel (right) to the actively creeping trace of the San Andreas fault. Aftershocks in the dense cluster of events around the hypocenters of the main shock are plotted as crosses (many were "lost" because of superposition). Aftershocks that lay northeast of the rift zone (more than 3.3 km northeast of the active trace) are plotted as large X's. Other aftershocks are plotted as solid circles.

a small shallow region containing the hypocenter of the main shock and lying within the San Andreas rift zone. Most of the remaining 20% of the aftershocks were distributed along two lines: the most prominent of these nearly coincides with the actively creeping strand of the fault near the southwest side of the rift zone; the other, which is parallel to the first, lies a kilometer or two northeast of the northeastern side of the rift zone. Focal depths in both of these zones ranged from near-surface to about 13 km.

It appears that this sequence may represent the disruption of material that temporarily "locked" a portion of the fault in a region that otherwise was undergoing pervasive creep. Aftershocks outside the concentrated zone of hypocenters surrounding the hypocenter of the main shock would then be considered to result from accelerated movement along surfaces where creep had been arrested while the temporary lock held. This view of the Bear Valley aftershock sequence suggests that the creep normally observed in this region extends to a depth of at least 13 km and that creep is not confined to the most prominent actively creeping strand of the fault.

The crustal model used in hypocenter determinations for the Bear Valley aftershocks was derived from two calibration shots, one set off near each end of the portable network. Large differences in the thickness of low-velocity near-surface rocks on opposite sides of the fault zone were taken into account by introducing appropriate traveltime corrections at individual stations. Only stations within 35 km of the epicenters were used in the hypocenter determinations in order to reduce the influence of the poorly established lower crustal layers on the calculation of focal depths. The crustal model used in determining the Bear Valley hypocenters was nearly the same as that for the Bay Area telemetered network.

Aftershocks of the 1966 Parkfield-Cholame earthquake

A detailed study of the aftershocks of the June 27, 1966, Parkfield–Cholame earthquake (Fig.2) was undertaken by N.C.E.R. in an attempt to establish the spatial relationship of the aftershocks to the zone of surface fracturing that accompanied the earthquake (Brown et al, 1967; Eaton et al., 1969). The initial objective of the work was to determine whether the aftershocks might reveal the slip surface over which movement occurred at the time of the magnitude 5.5 main shock and, if so, to determine the underground extent, particularly the lower limit, of the slip surface.

The field experiment was designed for maximum resolution in locating hypocenters beneath the southeastern half of the zone of surface fracturing. In that region, the 8 N.C.E.R. portable stations initially available were deployed in a circular cluster, with a diameter of about 20 km (Fig.11), centered on the end of the fractured zone and lying immediately southeast of the permanent N.C.E.R. station, Gold Hill (*GH*).

Recording in this region was begun early on July 1, 1966, about 70 h after the main shock, and it was continued until September 15, 1966. During the first three weeks of July, the Earthquake Mechanism Laboratory of E.S.S.A. operated five portable stations similar to the N.C.E.R. stations in a network around the preliminary instrumental epicenter of the main shock at the northwest end of the fractured zone (Fig.11). During September, this part of the aftershock region was again brought under reasonably adequate

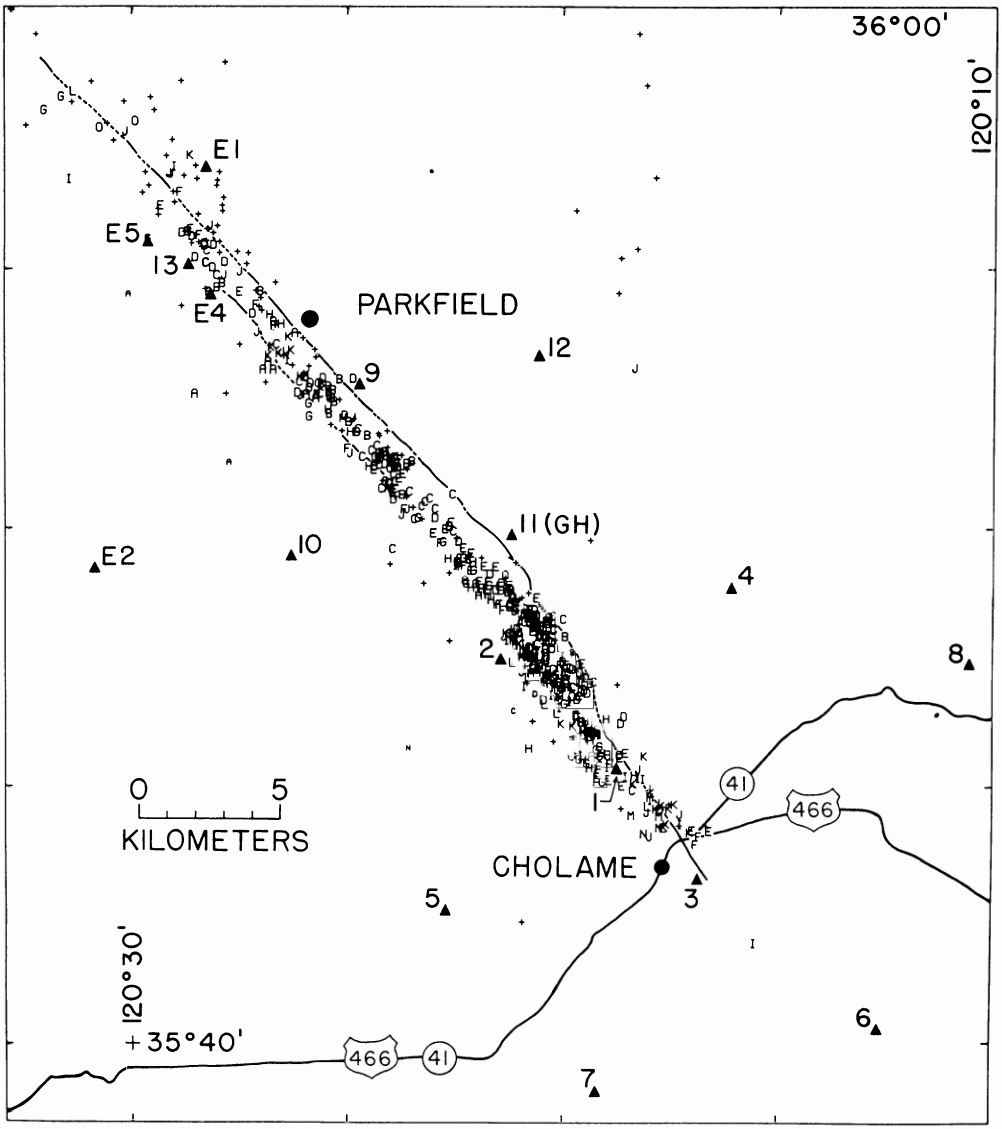

Fig.11. Aftershocks of the 1966 Parkfield–Cholame, California, earthquake. Stations of the portable network are indicated by triangles. Stations *E1* through *E5* were operated by the Earthquake Mechanism Laboratory of E.S.S.A.; the others by N.C.E.R. Zones of surface fracturing that accompanied the main shock and the aftershock sequence are shown as heavy solid and broken lines extending from the upper left to station *3*. The letter symbol that shows the epicenter of an aftershock also indicates its focal depth: 0–1 km = *A*, 1–2 km = *B*, and so on. Aftershocks for which focal depths could not be determined are plotted as crosses.

surveillance when 5 stations were added to the N.C.E.R. network to extend it toward the northwest. For earthquakes of magnitude 1.5 and larger, first P arrivals generally could be read at the University of California station at Priest, 44 km northwest of Gold Hill. When available, data from these supplementary stations were added to those from the N.C.E.R. network to extend coverage to the northwestern half of the epicentral region.

To attain the desired precision in hypocenter location, it was necessary to develop an adequate local crustal model, especially for the highly variable uppermost part of the crust, in the region occupied by the network. Two short refraction profiles parallel to and on opposite sides of the fault were run through the network in early September 1966. The northeastern one ran from near station *12*, past station *4*, to about midway between stations *6* and *8*. The southwestern one ran from near station *10*, past station *5*, to just east of station *7*. The constrasting velocity–depth models so determined are shown in the upper part of Fig.12 (S.W. Stewart and M.E. O'Neill, written personal communication). The lower two boundaries and velocities, which are common to both models, were derived from long seismic-refraction profiles from a shotpoint about 30 km west of Parkfield (Eaton, 1966). For computing traveltimes and derivatives of traveltimes with respect to the hypocentral coordinates as required in HYPOLAYR, crustal model 1 was used for stations southwest of the fault zone and crustal model 2 was used for stations northeast of the fault zone. This procedure neglects lateral refraction of rays passing through the fault zone (from one model to the other) and is a reasonable approximation only for foci lying on the surface dividing the two structures.

The epicenters of more than 600 aftershocks that were located are concentrated in a narrow zone just southwest of the zone of surface fracturing

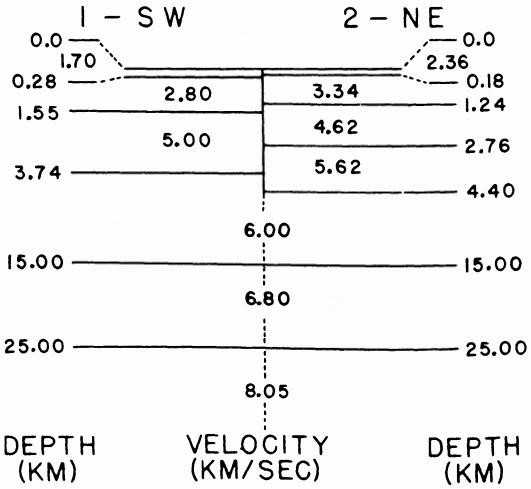

Fig.12. Dual crustal model used in the analysis of the Parkfield–Cholame aftershocks.

(Fig.11). The quality of hypocenter determination was considerably better, and the threshold for reliable detection of aftershocks was considerably lower (magnitude 0.5 vs. 1.5), for events along the southeastern half than along the northwestern half of the aftershock region.

To establish the orientation of the zone of aftershock sources and to provide a measure of the concentration of hypocenters along it, a reference plane was fitted by least squares to the three dimensional pattern of well located aftershock hypocenters. Such hypocenters were defined as ones for which: (1) the focal depth was not constrained; (2) the number of stations in the solution was at least 5; (3) the mean deviation of the residuals of observed arrival times with respect to the calculated ones was less than 0.1 second; and (4) the standard errors in both horizontal hypocentral coordinates were less than 2.5 km. For the first fitting, all 483 well located hypocenters within 10 km of the zone of surface fracturing were included. The standard deviation in the horizontal distance of hypocenters from the plane was 0.7 km. To refine the fit, the 9 well located events that lay more than 2 standard deviations from the first plane were rejected and the reference plane was refitted to the remaining 474 hypocenters. The final reference plane strikes N39°W and dips 86° toward the southwest. The standard deviation in the horizontal distance of hypocenters from the plane is 0.5 km. In Fig.13 the hypocenters of the well located aftershocks are projected onto a vertical plane perpendicular to the strike of the fitted plane.

The distribution of aftershocks along the fault is shown in Fig.14, where all events with epicenters within 10 km of the surface trace of the reference plane are projected onto a vertical plane through that trace.

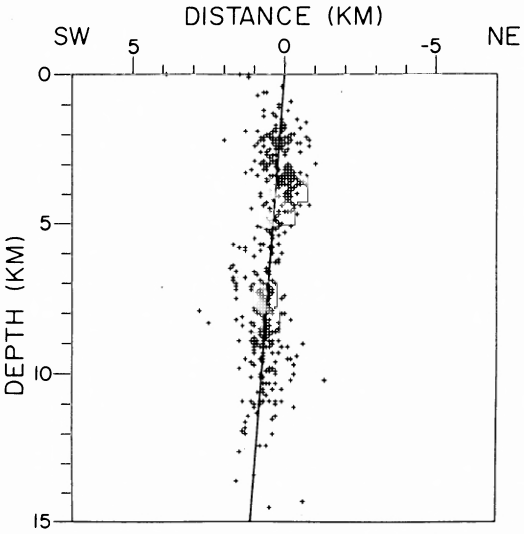

Fig.13. Hypocenters of well located Parkfield–Cholame aftershocks projected onto a vertical plane perpendicular to the surface trace of the reference plane fitted by least squares to the well located hypocenters. The reference plane is indicated by the solid line.

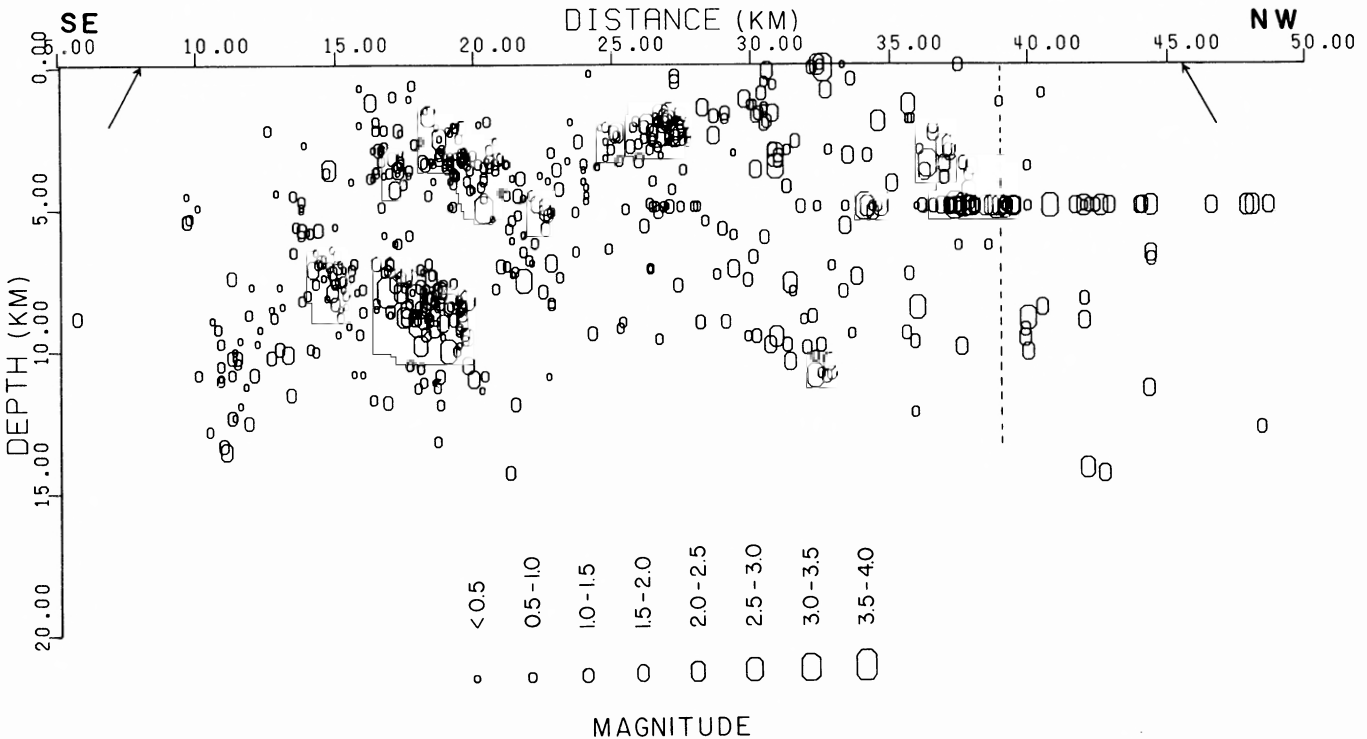

Fig.14. Hypocenters of Parkfield–Cholame aftershocks projected onto a vertical plane parallel to the surface trace of the reference plane fitted by least squares to the well-located hypocenters. The epicenter of the main shock is marked by the dashed vertical line at the northwest end of the aftershock zone, and the limits of the zone of surface fracturing are indicated by arrows. The concentration of hypocenters at a depth of 5 km at ranges of 35–50 km should be disregarded: inadequately recorded aftershocks were constrained to that depth to permit their epicenters to be calculated. The origin of the "distance" axis is near station *6*.

Magnitudes of the aftershocks are indicated by the size of the plotted symbols. An apparent concentration of aftershocks at a depth of 5 km in the right half of the plot results from the assignment of a 5-km depth to events for which focal depth cannot be determined. The aftershocks are virtually restricted to the depth range 1–12 km. They are also concentrated in patches on the slip surface; other patches are entirely devoid of aftershocks.

Histograms showing the number of aftershocks as a function of focal depth for various thresholds of magnitude are presented in Fig.15 for the southeastern half of the aftershock zone (distance range of 5–25 km in Fig. 14). Peaks in the frequency of occurrence of aftershocks in depth ranges 3–4 km and 8–9 km are separated by a sharp minimum at 5–7 km. The height of the peak at 8–9 km, relative to that at 3–4 km, increases with an increase in threshold magnitude. The same phenomenon is shown in somewhat different terms in Fig.16, where the number of aftershocks N larger than magnitude M are plotted versus M for each 2-km interval of focal depth from 2 to 14 km. In these graphs, the number of events in each 0.2 unit range in magnitude was plotted at the center of the range, and lines (log $N = a + bM$) were drawn by inspection through the points for $M \geq 0.5$. The value of $-b$ decreases from 1.03 for the interval 2–4 km to a minimum of 0.61 for the interval 8–10 km and then increases again for greater depths. It is difficult to judge whether this variation in b stems from some accidental irregularity in the slip-surface geometry, from some local peculiarity in the rock types in contact across the slip surface, or from depth-controlled variations in the behavior of rocks composing the earth's crust.

First-motion patterns from a very large majority of the aftershocks are compatible with right-lateral strike-slip displacements on the fault surface defined by the distribution of hypocenters. In most cases, however, the data are insufficient to establish the fault and auxiliary planes with precision. Accordingly, the hypocentral zone was divided into a number of

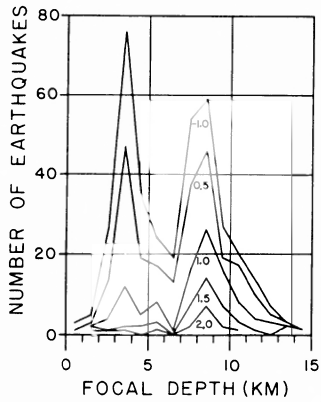

Fig.15. Histograms showing the distribution of aftershocks as a function of focal depth in the well-instrumented southeastern half of the Parkfield–Cholame aftershock region. Separate curves are drawn for various magnitude thresholds.

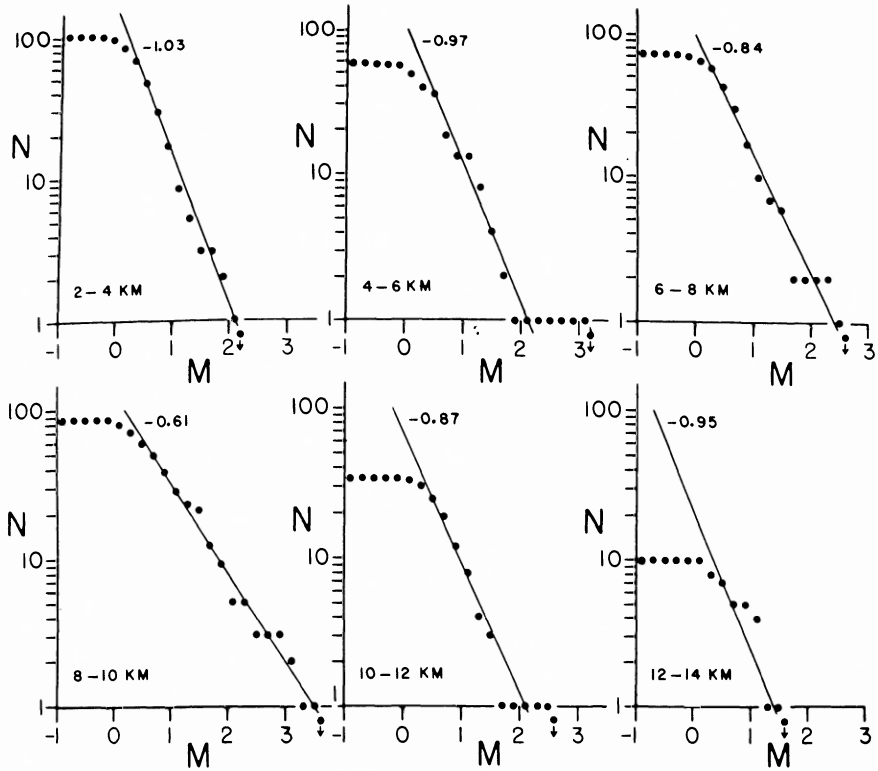

Fig.16. Frequency vs. magnitude plots, for various ranges of focal depth, of aftershocks from the well-instrumented southeastern half of the Parkfield–Cholame aftershock region. *N* is the number of earthquakes with magnitudes greater than *M*. The point above the arrow indicates the magnitude of the largest earthquake in each depth interval.

sections and composite first-motion diagrams from the aftershocks in each section were prepared. In Fig.17 the first motions from all events in section 4 (21–25 km distance range in Fig.14) are plotted in an equal-area projection of the lower half of the focal sphere. A pair of orthogonal planes representing the fault and auxiliary planes are well established by the data. We can safely identify the plane striking N41°W and dipping 88° southwest as the fault plane because it agrees so closely with the plane fitted to the well located hypocenters (N39°W, 86°SW). The steep dip of the auxiliary plane indicates that the slip vector was nearly horizontal; and the distribution of compressional and dilatational quadrants shows that the displacement was right-lateral, in agreement with observed surface displacements as well as with the gross behavior of the San Andreas fault.

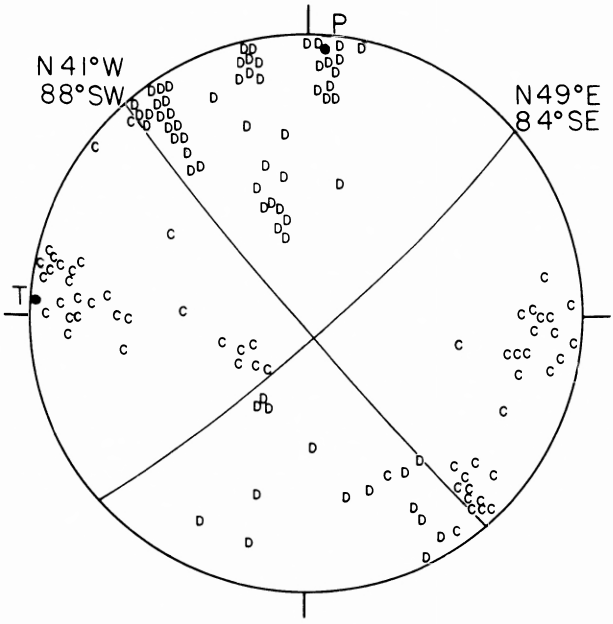

Fig.17. Composite first-motion plot of P waves from Parkfield–Cholame aftershocks within the distance range 21–25 km along the fault (see Fig.14). *C*'s and *D*'s indicate compressional and dilatational first motions, respectively. *T* and *P* denote the tension and pressure axes, respectively, of a fault plane solution that is compatible with first motions from all of the aftershocks on this section of the fault.

CONCLUDING OBSERVATIONS

Earthquakes along the San Andreas fault system in central California are limited to focal depths of 15 km or less and very few are deeper than 12 km. Although difficult to document convincingly, there appears to be a transition from "granitic" (6.0 ± km/sec) rocks of the upper crust to intermediate velocity (6.8 ± km/sec), possibly gabbroic, rocks of the lower crust at such depths in this region, where the total thickness of the crust is about 25 km.

The thickness of the lithospheric plates sliding past one another along the San Andreas fault system is probably substantially greater than that of the crust alone, perhaps 50 km or more. Accordingly, as Isacks et al. (1968) have pointed out, relative movement between these two plates in the lower crust and upper mantle is occurring without attendant earthquakes.

REFERENCES

Allen, C.R., St.-Amand, P., Richter, C.F. and Nordquist, J.M., 1965. Relationship between seismicity and geologic structure in the southern California region. Seismol. Soc. Am. Bull., 55: 753–797.

Bolt, B.A., Lomnitz, C. and McEvilly, T.V., 1968. Seismological evidence on the tectonics of central and northern California and the Mendocino escarpment. Seismol. Soc. Am. Bull., 58: 1725–1767.

Brown Jr., R.D. and Wallace, R.E., 1968. Current and historic fault movement along the San Andreas fault between Paicines and Camp Dix, California. In: W.R. Dickinson and A. Grantz (Editors), Proc. Conf. Geol. Sci., 11: 22–41. Andreas Fault System - Stanford Univ. Publ. Univ. Ser., Feol. Sci., 11: 22–41.

Brown Jr., R.D., Vedder, J.G., Wallace, R.E., Roth, E.F., Yerkes, R.F., Castle, R.O., Waananen, A.O., Page, R.W. and Eaton, J.P., 1967. The Parkfield–Cholame earthquakes of June–August 1966. U.S. Geol. Surv. Profess. Paper, 579,

Eaton, J.P., 1966. Crustal structure in northern and central California. In: E. Bailey (Editor), Geology of Northern California - Calif. Dept. Nat. Resources, Div. Mines, Bull., 190: 419–426.

Eaton, J.P., 1969. HYPOLAYR - a computer program for determining hypocenters of local earthquakes in an earth consisting of uniform flat layers over a half space. U.S. Geol. Surv., Open File Rept.

Eaton, J.P., O'Neill, M.E. and Murdoch, J.N., 1969. Aftershocks of the 1966 Parkfield–Cholame, California earthquakes: a detailed study. Seismol. Soc. Am. Bull., in press.

Hill, M.L. and Dibblee Jr., T.W., 1953. San Andreas, Garlock, and Big Pine faults, California - a study of the character, history, and tectonic significance of their displacements. Bull. Geol. Soc. Am., 64: 443–458.

Hofmann, R.B., 1968. Geodimeter fault movement investigations in California. Calif. Dept. Water Resources, Bull., 116-6, 183 pp.

Isacks, B., Oliver, J. and Sykes, L.R., 1968. Seismology and the new global tectonics. J. Geophys. Res., 73: 5855–5899.

Larsen, R.L., Menard, H.W. and Smith, S.M., 1968. Gulf of California: a result of ocean-floor spreading and transform faulting. Science, 161: 781–783.

Le Pichon, X., 1968. Sea-floor spreading and continental drift. J. Geophys. Res., 73: 3661–3697.

Morgan, W.J., 1968. Rises, trenches, great faults, and crustal blocks. J. Geophys. Res., 73: 1959–1982.

Radbruch, D.H., 1968. New evidence of historic fault activity in Alameda, Contra Costa, and Santa Clara Counties, California. In: W.R. Dickinson and A. Grantz (Editors), Proc. Conf. Geol. Problems San Andreas Fault System - Stanford Univ. Publ., Univ. Ser., Geol. Sci., 11: 46–54.

Radbruch, D.H., Bonilla, M.G., and others, 1966. Tectonic creep in the Hayward fault zone, California. U.S. Geol. Surv. Circ., 525, 13 pp.

Rogers, T.H. and Nason, R.D., 1968. Active faulting in the Hollister area. In: R. Dickinson and A. Grantz (Editors), Proc. Conf. Geol. Problems San Andreas Fault System - Stanford Univ. Publ. Univ. Ser., Geol. Sci., 11: 42–45. Univ. Ser., Geol. Sci., 11: 42–45.

Steinbrugge, K.V. and Zacher, E.G., 1960. Creep on the San Andreas fault - fault creep and property damage. Seismol. Soc. Am. Bull., 50: 389–396.

Sykes, L.R., 1968. Seismological evidence for transform faults, seafloor spreading, and continental drift. In: R.A. Phinney (Editor), Proceedings of NASA Symposium, History of the Earth's Crust. Princeton University Press, Princeton, N.J.

Tocher, D., 1960. Creep on the San Andreas fault - creep rate and related measurements at Vineyard, California. Seismol. Soc. Am. Bull., 50: 396–404.

Tocher, D., 1966. Fault creep in San Benito County, California (abstract). Geol. Soc. Am. Inc., Cordilleran Sect. - Seismol. Soc. Am. - Paleontol. Soc., Pacific Coast Sect., 62nd Ann. Meeting, Reno, Nev., 1966, Program, p.72.

Wentworth, C., 1968. Upper Cretaceous and Lower Tertiary strata near Gualala, California, and inferred large right lateral slip on the San Andreas fault. In: William R. Dickinson and A. Grantz (Editors), Proc. Conf. Geol. Problems San Andreas Fault System - Stanford Univ. Publ., Univ. Ser., Geol. Sci., 11: 130–143.

Wilson, J.T., 1965. Transform faults, ocean ridges, and magnetic anomalies southwest of Vancouver Island. Science, 150: 482–485.